optica

Wavefront-shaping-based correction of optically simulated cataracts

AUGUSTO ARIAS* AND PABLO ARTAL

Laboratorio de Óptica, Universidad de Murcia, Campus de Espinardo (Edificio 34), Murcia 30100, Spain
**Corresponding author: augusto.arias@um.es*

Received 12 June 2019; revised 8 November 2019; accepted 26 November 2019 (Doc. ID 369662); published 3 January 2020

Cataracts is a common ocular pathology where the crystalline lens tends to become opaque, degrading the quality of the retinal images because of the increase of both aberrations and scattering. In this work, we simultaneously generated and optically corrected the effects of cataracts in an optical bench by using a liquid crystal device spatial light modulator. The correction was carried out by implementing a feedback-based wavefront shaping technique with different spatial resolutions of the corrector phase maps. Its benefits were evaluated through objective and subjective descriptors of the quality of vision. The analysis of the experimental results, in addition to numerical calculations of the uncorrected and corrected ocular point spread functions, allowed us to understand the limitations of the technique and to present a strategy to overcome it for future *in vivo* applications.

https://doi.org/10.1364/OPTICA.7.000022

1. INTRODUCTION

Cataracts is the first cause of reversible blindness in the world [1]. This pathology is related to the increase of the backward and forward intraocular scattering due to the oxidative stress in the proteins that compose the crystalline lens [2]. Cataracts are commonly graded through the observation of the lens opacities [3] (i.e., the backward scattering), but their impact on the quality of vision is determined by the amount of the forward scattered light (or straylight). Their effects on the retinal images are blurring and reduction of contrast.

The current cataract treatment is surgery wherein the opaque lens is extracted and replaced by an intraocular lens. Despite the simplicity of this surgical procedure, it poses possible side effects such as corneal edema, increase of intraocular pressure, infection, uveitis, and retinal detachment, among others [4]. Moreover, this procedure is not recommendable in some cases such as the congenital cataract in infants [5]. Those contraindications and complications would be avoided by using a purely optical correcting approach.

Adaptive optics has been applied to improve the quality of retinal images; however, the performance of Hartmann–Shack sensors in estimating the ocular wavefront is limited due to the high amount of straylight present in the cataractous eyes [6]. Therefore, some unconventional imaging techniques have been proposed and experimentally tested to optically compensate for the effects of the cataracts. Miller *et al.* [7] retrieved and compensated the phase map of an *ex vivo* cataractous lens by using holography and considering a single pass through the ocular media. Liu *et al.* [5] more recently retrieved the focal point through an *ex vivo* cataractous lens with time-reversing optical phase conjugation.

Light could be focused through a scattering media, such as the cataractous lens, by implementing the feedback-based wavefront shaping (WS) technique [8]. It is based on the local manipulation of the wavefront to produce constructive interference at a selected spatial position. For the *in vivo* application of this technique it is necessary to consider that the optical response of the human eye is conventionally acquired after a double-pass propagation of the testing beam through the ocular media [9]. However, vision occurs after the first pass. Thus, the performance of WS will be influenced by the quality of the imaged point at the retina. It could be generated by using several approaches [10] such as ultrasound (used by Liu *et al.*), fluorescence, and all-optical [11].

In this work, the performance of WS for the correction of the effects of cataracts was experimentally evaluated in an optical bench by assuming that the light from a perfect point source passes through the ocular media one time. Moreover, this approach avoids the influence of some factors that could affect the performance of the technique such as the tear film stability, eye movements, and accommodation. Therefore, the experimental results can be interpreted as the highest benefit provided by this technique.

The effects of three different amounts of straylight, associated with three degrees of cataracts, were simultaneously reproduced and corrected by using a liquid crystal device on silicon spatial light modulator (LCoS-SLM). The benefits of the technique were evaluated by using objective and subjective descriptors of the quality of vision. Moreover, the uncorrected and corrected wide-angle point-spread functions (PSFs) where numerically calculated. Finally, a

strategy to improve the quality of the correction to extended images is proposed.

2. METHODS

A. Optical Setup

The optical setup is shown in Fig. 1. It is designed to simultaneously reproduce and correct the effects of cataracts based on a double pass through a LCoS-SLM (PLUTO; Holoeye, AG, Germany). The area of the LCoS is divided in two halves to display the testing (or correcting) and aberrated phase maps in the first and second half, respectively. The size of both phase maps (N) is 800 pixels. The halves are conjugated by a telescope with unitary magnification that is composed of a single lens and two mirrors. The Fraunhofer pattern of the exit pupil, after the second pass, is acquired by an electron-multiplying CCD camera (Luca; Andor, Belfast, UK) when the first half is illuminated by an expanded and collimated laser beam (wavelength $\lambda \equiv 532$ nm) with horizontal polarization.

The inherent aberrations of the optical setup (i.e., those not programmed in the LCoS) were compensated to aim the WS correction on the effects of induced straylight. The sources of such aberrations are the silica plate that supports the cells of liquid crystal in the LCoS [12], the oblique incidence of the beam in the LCoS, and the decentered illumination of the lens that conjugates both halves of the modulator. We implemented a hill-climbing algorithm [13] to increase the Strehl ratio by decomposing the correcting phase map in Zernike polynomials [14] from the secnd to the fifth order. After this correction, the Strehl ratio was enhanced 2.8-fold.

The overlapping between the zero-order diffraction, understood as the undiffracted light after the pass by the LCoS, and the scattered light patterns could confuse further analyses on the Fraunhofer pattern. Therefore, in order to suppress the zero-order diffraction and to manipulate the size of the aperture, binary phase gratings were added to the phase maps displayed on the LCoS. The

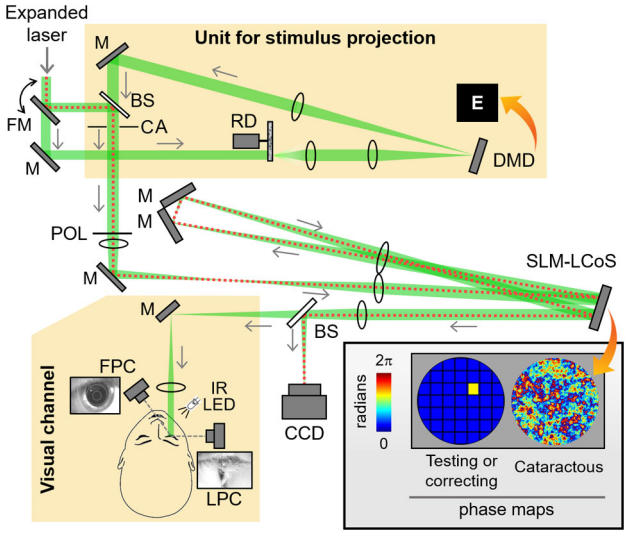

Fig. 1. Experimental setup for the simultaneous generation and compensation of the effects of intraocular straylight. Label descriptions: FM, flip mirror; M, mirror; RD, rotating diffuser; BS, beam splitter; CA, circular aperture; POL, linear polarizer; IR LED, infrared light-emitting diode; FPC and LPC, frontal and lateral pupil cameras, respectively. The red dotted line depicts the path of the beam during the feedback-based WS correction.

depth of modulation and period of the gratings were π radians and two pixels. After each pass through the LCoS, the first-order diffraction was filtered.

The feedback-based WS was implemented following the stepwise sequential algorithm [15]. The testing phase map was divided in regular segments where the phase of each segment was gradually changed between 0 to 2π radians in twelve steps, selecting the phase value (φ) that maximizes the intensity at the target. The latter corresponds to the grain of speckle with the highest energy, where ballistic photons are generally reaching the camera at the Fraunhofer pattern. The intensity and phase data for each segment were fitted to a cosine function to accurately estimate φ as its phase shift, minimizing the effect of the noise introduced by the CCD device. Moreover, φ values were discretized in 16 values between 0 to 2π radians leading to a theoretical diffraction efficiency of the correcting phase map of 98.7%. Seven sizes of the segment were used for the corrections of each amount of straylight: 80, 50, 40, 32, 25, 20, and 16 pixels of the LCoS-SLM that correspond to 274, 171, 137, 110, 86, 69, and 55 μm in the generated artificial pupil, respectively.

Once the correction is completed, its effects on the extended and spatially incoherent images were evaluated by using a stimulus projection unit (see Fig. 1). In this unit, high-contrast objects (e.g., bars or optotypes) are generated by a digital micromirror device (DMD, ViALUX 1100; Texas Instruments Inc., USA) illuminated by the same laser beam used in the correction stage. A rotating diffuser breaks the spatial coherence of the beam. A set of lenses translate the object to the image plane at the camera following the double pass through the LCoS-SLM.

Additionally, a visual channel was incorporated for the subjective evaluation of the correction where the entrance pupil of the subject's eye is conjugated with the LCoS-SLM by a telescope with a magnification of 0.43. Thus, the size (ϕ) of the projected artificial pupil was 2.7 mm. The transversal and axial position of the eye's pupil is monitored by means of two CMOS cameras [frontal pupil camera (FPC) and lateral pupil camera (LPC) in Fig. 1] together with an infrared LED while the subject's head is stabilized by a chin and forehead rest.

B. Calculation of Cataractous Phase Maps

The optical effects of the cataractous ocular media were reproduced by modelling the ocular transmittance (Ae^{iW}) according to the methodology introduced in Ref. [16]. A is a circular aperture with diameter ϕ acting as the iris. W is a pseudo-self-replicant surface calculated as the inverse cosine transform (IDCT) of the product between the $F(f_i, f_j)$ function and the standard normally distributed random values in the matrix R with dimension N:

$$W = \sum_{i=o}^{N-1}\sum_{j=0}^{N-1} F(f_i, f_j) R_{ji} \cos\left(\frac{\pi \phi f_i}{N} i'\right) \cos\left(\frac{\pi \phi f_j}{N} j'\right), \tag{1}$$

where f_i and f_j are the spatial frequencies of the horizontal and vertical cosine modes, respectively.

F is a power law function with B and β parameters for the control of the amplitude and fractal dimension, respectively,

$$F(f_i, f_j) = B(f_i^2 + f_j^2)^{\beta/2}. \tag{2}$$

Thus, the B and β values are numerically optimized to adjust the angular course of the PSF produced by the modelled transmittance to the total glare function suggested by the Commission

International d'Eclairage (CIE) [17]. The PSF associated to each wavefront were calculated using the fast Fourier transform [18].

The amount of straylight s is defined as $\theta^2 \times \mathrm{PSF}(\theta)$, where θ corresponds to the retinal angle. It is generally reported in a logarithmic scale, i.e., $\mathrm{Log}_{10}(s)$. In this work, $\mathrm{Log}_{10}(s)$ values of 1.75, 2.00, and 2.25 at 3.5 deg were generated, which can be clinically associated to nuclear cataracts ranked 3, 4, or higher in the Lens Opacities Classification System III (LOCS-III) [3].

Considering the given experimental parameters (N, λ, and ϕ), the calculated B and β values that reproduce the effects of the lowest amount of straylight [i.e., $\mathrm{Log}_{10}(s) = 1.75$] are 5.30 μm and −1.11, respectively. Figure 1 (inset) shows the calculated phase map. The additional s amounts were reproduced by manipulating the amplitude of the previously calculated phase map, taking advantage of the following linear relationship between the logarithmic values of s and B:

$$\mathrm{Log}_{10}(s) = 1.744\mathrm{Log}_{10}(B) + 0.487. \tag{3}$$

C. Evaluation of the WS Correction

The impact of WS correction for each amount of straylight was assessed through the following objective and subjective metrics: the enhancement of the PSF (η), the logarithm of the visual Strehl ratio calculated on the modulation transfer function (LogVSMTF), the correlation coefficients (CC), and the visual acuity (VA).

η is calculated as the ratio between the optimized intensity at the target and the average of intensity around that position before the correction [8].

The LogVSMTF can account up to 86% of the variance in high-contrast visual acuity [19]. Its calculation includes a weighting of the radially averaged modulation transfer function (MTF) by the neural contrast sensitivity function [20] (NCSF):

$$\mathrm{LogVSMTF} = \mathrm{Log}_{10}\left[\frac{\sum_g \mathrm{MTF}(g)\mathrm{NCSF}(g)}{\sum_g \mathrm{MTF}_s(g)\mathrm{NCSF}(g)}\right], \tag{4}$$

where g is the spatial frequency and MTF_s corresponds to the MTF of the system without induced straylight.

The radially averaged MTFs were approximated to the average of the horizontal and vertical profiles, which were measured by implementing the four bar method [21]. The MTF profiles were discretized in 17 spatial frequencies from 3 to 80 cpd.

The CC, a good descriptor of the visual acuity in highly aberrated eyes [22], is used to quantify the similarity between the imaged optotypes through the system without (O) and with (I) uncorrected or corrected straylight. Mathematically, CC is defined as [23]

$$\mathbf{CC} = \frac{\sum_{i=1}^{M}\left(O_i - \bar{O}\right)\left(I_i - \bar{I}\right)}{\sqrt{\sum_{i=1}^{M}\left(O_i - \bar{O}\right)^2}\sqrt{\sum_{i=1}^{M}\left(I_i - \bar{I}\right)^2}}, \tag{5}$$

where M is the number of elements of the digitalized images. The metric is ranged from 0 to 1, the former when the images are completely uncorrelated and the latter when they are identical. CCs were calculated on black-on-white (BoW) and white-on-black (WoB) E optotypes with eight angular sizes ranged from 2.94 to 16.18 minarc. In the BoW polarity, optotypes are in the center of a white square that triples its size.

In addition to the previous objective metrics, the impact of the WS optimization on the spatial resolution of the human eye was assessed by directly measuring the VA. The measurements were performed in the right eye of three trained subjects, without any known ocular pathologies, whose age and refraction were as follows: S1, 34, sphere −1.98 D, cylinder −0.38 D; S2, 28, sphere −0.52 D, cylinder −0.17 D; and S3, 31, sphere −1.94 D, cylinder −0.28 D. The refractive error for each eye was corrected using the LCoS-SLM device. Low light conditions in the experimental room were used to prevent the occlusion of the artificial pupil by the natural one. VA was measured by implementing the "best parameter estimation by sequential testing" (known as BestPEST) [24] procedure with 45 trials. In each trial, the task of the subject was to determine the orientation of a tumbling E by typing the arrows of the keyboard. The stimuli were displayed by the DMD for 0.3 s after an acoustic signal. The size of optotypes were linearly spaced from 0.45 to 44.55 arcmin. The reported VA values, for each experimental condition, is the average of three successive measurements.

VA is generally affected by both quality and luminance of the image projected on the retina; however, there is a luminance range where the VA only depends on the former [25]. To focus the subjective evaluation exclusively on the quality of the retrieved images, the VA with the natural aberrations of each subject (except defocus) was preliminary assessed on a luminance range from 0.75 to 11.84 cd/m^2 using neutral density filters. The luminance was measured using a CMOS camera (DCC1545M; Thorlabs Inc., Germany) previously calibrated with a luminance meter (LS-100; Konica-Minolta Inc, Japan).

D. Numerical Simulation of WS Effect on the Wide-Angle PSF

The detailed experimental inspection of the generated PSF in its complete angular range (9.08 deg, approximately) is not possible because of the restricted dynamic range of the camera. Therefore, the impact of WS on straylight was evaluated through the numerical calculation of the uncorrected and corrected wide-angle PSFs for the three induced amounts of straylight, considering the experimental parameters. The propagation of the optical field was calculated using the fast Fourier transform [18].

3. RESULTS

A. Enhancement Factor

Regardless the induced amounts of straylight and the size of segments, the corrected PSFs corresponded to a diffraction-limited peak over a background of uncorrected scattering. Figure 2(a) shows a comparison between the uncorrected and corrected generated ocular PSFs.

The dependence of the η factor on the size of the segment for each generated amount of straylight is depicted in Fig. 2(b). The enhancement increases as s increases due to the reduction of the maximum intensity in the uncorrected PSF. A threshold of η was reached when the lowest induced straylight level [$\mathrm{Log}_{10}(s) \equiv 1.75$] was corrected with sizes of the segments lower than 69 μm.

B. Logarithm of Visual Strehl Ratio

Figure 3(a) shows a comparison among the uncorrected and best corrected (by using a size of segment of 55 μm) MTF profiles. As one would expect, the MTF is severely reduced as the induced straylight increases. For all sizes of the segment, WS improved the

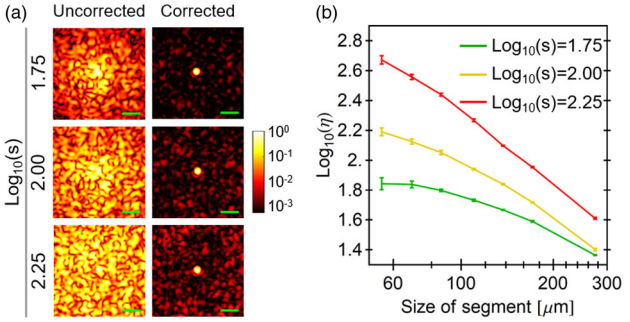

Fig. 2. (a) Normalized uncorrected and corrected (by using a size of segment of 110 μm) PSFs for each amount of straylight. Length of the green bar is 5 arcmin. (b) Enhancement factor as function of the size of the segment. Error bars are standard deviation.

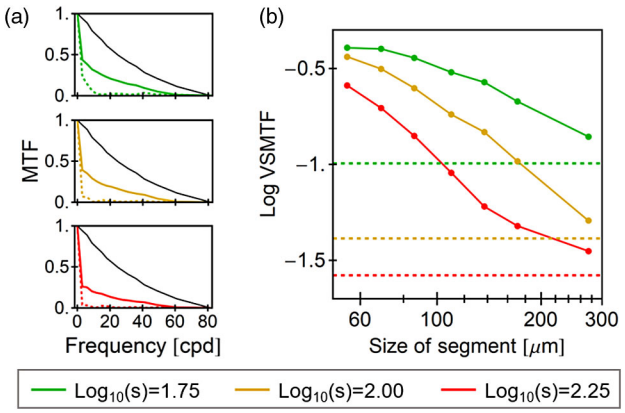

Fig. 3. (a) Comparison of the MTF profiles for the uncorrected (dashed line), corrected (continuous line), and without induced (black line) straylight. (b) LogVSMTF as function of the size of segment for each amount of straylight, depicting the uncorrected values with the dashed lines.

MTF values for spatial frequencies less than 60 cpd whose range has a visual impact. That improvement depends on the spatial resolution of the correcting wavefront, being higher when the size of the segment is reduced.

The WS impact on the LogVSMTF values for each amount of straylight is shown in Fig. 3(b). In the case of the high and medium straylight levels, the corrected LogVSMTF increases as the size of the segment decreases. However, a threshold was reached in the correction of the lowest straylight level [i.e., $\mathrm{Log}_{10}(s) \equiv 1.75$] for sizes of the segment lower than 69 μm, which is in line with the observed threshold of the η factor (see Fig. 2).

C. Correlation Coefficients

Figure 4(a) shows the effect of WS correction on the image of small- and largesized optotypes with two contrast polarities (WoB and BoW) for the three generated amounts of straylight. All corrected images have the same spatial resolution because of the morphology of the optimized PSFs.

The assessed CC values for the optotypes with both contrast polarities and several sizes are shown in Fig. 4(b). WS significantly impacts the CC values for the WoB optotypes, where the corrected values are almost 1. However, the scattering that remains uncorrected after the WS optimization adds a luminance veil

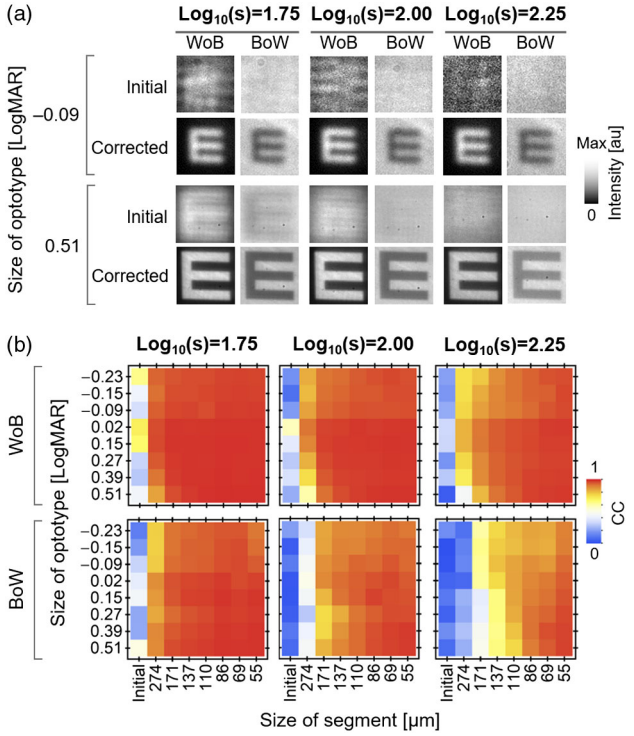

Fig. 4. (a) Uncorrected and corrected (by using a size of segment of 55 μm) small- and large-sized optotypes with both polarities. (b) Correlation coefficients as function of the size of the optotypes and segments for both polarities and the three induced amounts of straylight.

from the optotype itself that reduces the contrast of the optotypes, decreasing the CC values when the amount of straylight and the size of both the optotype and segment increases. That reduction of contrast is more evident in the corrected image of BoW optotypes whose CC values are notably lower than those in the WoB case.

D. Visual Acuity

The VA (in LogMAR units) without induced straylight as a function of stimulus luminance is shown in Fig. 5(a). The inter-subject average of the VA can be considered constant in the luminance range of the corrected stimulus, which is marked with the cyan line. The averaged VA in that range is -0.13 ± 0.02 LogMAR.

To equalize the luminance of the best corrected stimulus (i.e., the lowest size of the segments) for all amounts of straylight, the intensity was reduced by using neutral density filters with optical densities of 0.4 and 0.3 when the uncorrected and corrected VA was assessed for $\mathrm{Log}_{10}(s)$ amounts equal to 1.75 and 2.00, respectively. Figure 5(b) shows the WS impact on the inter-subject average of VA for different sizes of the segments.

In general, VA was enhanced by WS correction (i.e., the corrected values in LogMAR units were notably lower than uncorrected ones). For all straylight levels, the corrected VA will correspond to the value without induced straylight when the spatial resolution of the correcting wavefront is increased (i.e., the size of the segment is decreased). For a large size of segments, the corrected VAs were affected by the lack of contrast as in the case of the CC values.

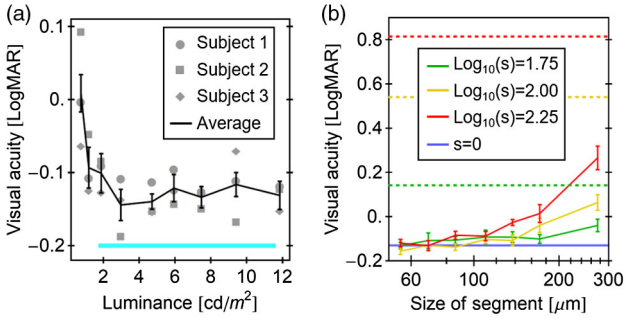

Fig. 5. (a) High-contrast visual acuity as function of the stimulus luminance. The cyan line depicts the luminance range of the corrected optotypes. (b) Comparison of inter-subject averaged visual acuity with uncorrected (dashed lines), corrected (continuous line) and without (blue line) straylight. Error bars are standard deviations.

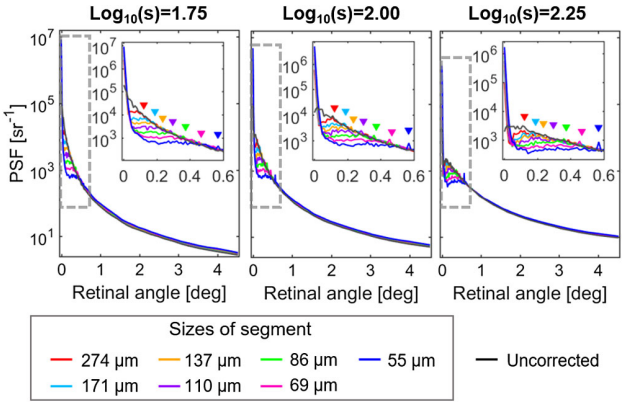

Fig. 6. Numerical calculation of the uncorrected and corrected radially averaged wide-angle PSFs.

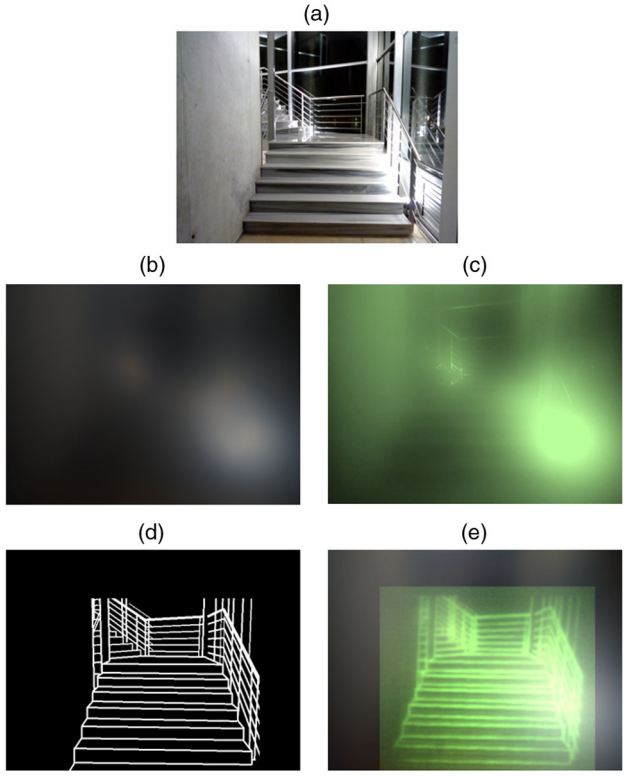

Fig. 7. Simulation of a scene seen through: (a) clear optics, (b) the advanced cataractous effects, and (c) their partial correction by WS. (d) Proposed simplification to lead (e) the increased contrast image.

E. Numerical Wide-Angle PSFs

The numerically calculated radially average of the uncorrected and corrected wide-angle PSFs are shown in Fig. 6 where the triangles mark the diffraction angle (ρ) associated to each segment size of the correcting wavefronts. The ρ angle is given by $\sin^{-1}(\lambda/b)$, where b is the size of segment. The impact of WS on the PSF is limited to the angular range of ρ where the light is spatially redistributed to form the central peak. Thus, while the protruding peak of the corrected PSFs deblurs the retinal images, the uncorrected straylight leads to a reduction of contrast.

4. DISCUSSIONS AND CONCLUSION

The performance of WS in the correction of three different amounts of straylight were experimental and numerically evaluated through objective and subjective metrics. Those effects, which can be associated to three levels of cataracts, were generated by calculating zero-thickness phase screens with random perturbations. The corrections were performed using seven sizes of the segments that compose the testing and correcting wavefronts.

The results initially allowed us to identify the optimal size of segment for the correction of a weak cataract state [i.e., $\text{Log}_{10}(s) \leq 1.75$]. It corresponds to 69 μm, according to the η and LogVSMTF measurements [see Figs. 2(b) and 3(b)], where a threshold was reached in both metrics. Therefore, the use of smaller segment increases would increase the correction time without a significant increment of the quality of the retinal images. For higher amounts of straylight, the spatial resolution of the correcting wavefronts must be increased in order to achieve a threshold of the η and LogVSMTF values.

WS significantly benefits both CC and VA values [Figs. 4(b) and 5(b)] while the scattering is not corrected (see Fig. 6). Thus, the effect of WS correction on the retinal images is basically deblurring, but the contrast still reduced. For a better understanding of this partial correction, Fig. 7 shows a physical simulation of its effect on the image of a real-life scenario [see Fig. 7(a)], which is composed of a stair with lamps around. The retinal image of an eye with advanced cataracts [i.e., $\text{Log}_{10}(s) \equiv 2.25$] is affected by blurring and loss of contrast and intensity as shown in Fig. 7(b). If the scene is seen through a corrector based on WS, it will look deblurred and brighter, but the contrast will still be reduced due to the straylight from the glare sources (e.g., the lamps or their specular reflections) as depicted in Fig. 7(c). Hence, this partial correction could not offer a visual benefit. The methodology of this simulation is explained in Supplement 1.

The contrast of the corrected image projected on the retina can be increased by incorporating the WS corrector to an augmented reality setup. In this way, the scene is recorded and digitally processed in order to identify its key information and to avoid the effect of the glare sources. Then, the simplified and corrected image is projected on the retina, being imposed to the retinal image affected by the cataracts in order to preserve some insights of the environment (e.g., surrounding luminance level). An example of the proposed simplification on Fig. 7(a) is shown in Fig. 7(d). In this case, an edge-detection operation was simulated, creating a

binary image where the structure of the stairs could be easily identified. For the experimental demonstration, this simplified image was displayed in the stimulus projection unit of the developed instrument (see Fig. 1) to be recorded under the partially compensated effects of straylight [$\mathrm{Log}_{10}(s) \equiv 2.25$] using a binning size of 55 μm. Figure 7(e) shows the retrieved simplified stimulus that was digitally added to Fig. 7(b), demonstrating the improvement of its contrast.

The reported metrics are useful to understand the visual impact of *in vitro* or *in vivo* implementations of unconventional approaches for the correction of cataracts. For example, Liu *et al.* [5] corrected the PSF of an artificial cataractous eye, composed of an *ex vivo* human opaque lens in front of a cow retina, by using WS based on optical phase conjugation. According to the authors, after the correction, "the average intensity inside the focus is 13 times higher than the average intensity of the surrounding background." In our experience, the values of that metric for the three reproduced amounts of straylight corrected with the lowest size of segment (274 μm) corresponded to 136 ± 3 times, $\mathrm{Log}_{10}(s) \equiv 1.75$; 85 ± 3 times, $\mathrm{Log}_{10}(s) \equiv 2.00$; and 65 ± 3 times, $\mathrm{Log}_{10}(s) \equiv 2.25$. As those values are higher than 13, the benefits on the quality of vision of the double-pass correction performed by Liu *et al.* would be lower than that assessed in our optical bench. Moreover, the assembled optical bench can be easily adaptable to test the performance of WS in a symmetric or asymmetric double pass through the ocular media, allowing us to find the most proper way for further *in vivo* applications.

The accuracy of the adopted methodology to reproduce the ocular PSF, based on a zero-thickness phase screen, was previously demonstrated [16]. However, this approach is not suitable to quantify the field of view of the corrected eye or the impact of the eye movements on the quality of the correction, which would be dictated by the optical memory effect [26]. This effect is a consequence of the multiple scattering events inside the turbid volume. It has been widely studied in highly scattering samples but not for cataractous lens.

In conclusion, the highest benefits (according to the spatial resolution of the compensating wavefront) of the WS correction of the effects of three levels cataracts were evaluated. Although WS significantly improves the spatial resolution of the corrected images, the contrast was still reduced. This limitation could be overcome in the future by digital simplification of the scenarios to be projected through the WS corrector.

Funding. H2020 European Research Council (AdG−2013−339228 SEECAT); Secretaría de Estado de Investigación, Desarrollo e Innovación (FIS2013-41237-R); Fundación Séneca (19897/GERM/15); Spanish Government (FPI-BES-2014-070427).

See Supplement 1 for supporting content.

REFERENCES

1. R. R. A. Bourne, S. R. Flaxman, T. Braithwaite, M. V. Cicinelli, A. Das, J. B. Jonas, J. Keeffe, J. H. Kempen, J. Leasher, H. Limburg, K. Naidoo, K. Pesudovs, S. Resnikoff, A. Silvester, G. A. Stevens, N. Tahhan, T. Y. Wong, and Y. Zheng, "Magnitude, temporal trends, and projections of the global prevalence of blindness and distance and near vision impairment: a systematic review and meta-analysis," Lancet. Glob. Heal. **5**, e888–e897 (2017).
2. R. Michael and A. J. Bron, "The ageing lens and cataract: a model of normal and pathological ageing," Philos. Trans. R. Soc. B. **366**, 1278–1292 (2011).
3. L. T. Chylack, J. K. Wolfe, D. M. Singer, M. C. Leske, M. A. Bullimore, I. L. Bailey, J. Friend, D. McCarthy, and S.-Y. Wu, "The lens opacities classification system III," Arch. Ophthalmol. **111**, 831 (1993).
4. E. Chan, O. A. R. Mahroo, and D. J. Spalton, "Complications of cataract surgery," Clin. Exp. Optom. **93**, 379–389 (2010).
5. Y. Liu, Y. Shen, H. Ruan, F. L. Brodie, T. T. W. Wong, C. Yang, and L. V. Wang, "Time-reversed ultrasonically encoded optical focusing through highly scattering ex vivo human cataractous lenses," J. Biomed. Opt. **23**, 010501 (2018).
6. T. Mihashi, Y. Hirohara, K. Bessho, N. Maeda, T. Oshika, and T. Fujikado, "Intensity analysis of Hartmann-Shack images in cataractous, keratoconic, and normal eyes to investigate light scattering," Jpn. J. Ophthalmol. **50**, 323–333 (2006).
7. D. Miller, J. L. Zuckerman, and G. O. Reynolds, "Phase aberration balancing of cataracts using holography," Exp. Eye Res. **15**, 157–160 (1973).
8. I. M. Vellekoop and A. P. Mosk, "Focusing coherent light through opaque strongly scattering media," Opt. Lett. **32**, 2309–2311 (2007).
9. J. Santamaría, P. Artal, and J. Bescós, "Determination of the point-spread function of human eyes using a hybrid optical-digital method," J. Opt. Soc. Am. A **4**, 1109–1114 (1987).
10. R. Horstmeyer, H. Ruan, and C. Yang, "Guidestar-assisted wavefront-shaping methods for focusing light into biological tissue," Nat. Photonics **9**, 563–571 (2015).
11. G. Stern and O. Katz, "Noninvasive focusing through scattering layers using speckle correlations," Opt. Lett. **44**, 143–146 (2019).
12. J. Harriman, A. Linnenberger, and S. Serati, "Improving spatial light modulator performance through phase compensation," Proc. SPIE **5553**, 58–67 (2004).
13. Y. Liu, J. Ma, B. Li, and J. Chu, "Hill-climbing algorithm based on Zernike modes for wavefront sensorless adaptive optics," Opt. Eng. **52**, 016601 (2013).
14. L. N. Thibos, R. A. Applegate, J. T. Schwiegerling, and R. Webb, and VSIA Standards Taskforce Members, "Standards for reporting the optical aberrations of eyes," J. Refract. Surg. **18**, S652–S660 (2002).
15. I. M. Vellekoop and A. P. Mosk, "Phase control algorithms for focusing light through turbid media," Opt. Commun. **281**, 3071–3080 (2008).
16. A. Arias, H. Ginis, and P. Artal, "Light scattering in the human eye modelled as random phase perturbations," Biomed. Opt. Express **9**, 2664–2670 (2018).
17. J. J. Vos, B. L. Cole, H.-W. Bodmann, E. Colombo, T. Takeuchi, and T. J. T. P. van den Berg, *CIE Equations for Disability Glare* (2002).
18. D. Mas, J. Garcia, C. Ferreira, L. M. Bernardo, and F. Marinho, "Fast algorithms for free-space diffraction patterns calculation," Opt. Commun. **164**, 233–245 (1999).
19. A. Ravikumar, E. J. Sarver, and R. A. Applegate, "Change in visual acuity is highly correlated with change in six image quality metrics independent of wavefront error and/or pupil diameter," J. Vis. **12**(10):11 (2012).
20. A. B. Watson and A. J. Ahumada, "A standard model for foveal detection of spatial contrast," J. Vis. **5**(9):6–740 (2005).
21. G. D. Boreman and S. Yang, "Modulation transfer function measurement using three- and four-bar targets," Appl. Opt. **34**, 8050–8052 (1995).
22. G. Yoon, "The use of metrics and adaptive optics to evaluate different correction strategies for highly aberrated eyes," in *Wavefront Congress* (2008).
23. J. L. Rodgers and W. A. N. Wander, "Thirteen ways to look at the correlation coefficient," Am. Statist. **42**, 59–66 (1988).
24. H. R. Lieberman and A. P. Pentland, "Microcomputer-based estimation of psychophysical thresholds: the best PEST," Behav. Res. Methods Instrum. **14**, 21–25 (1982).
25. S. Marcos, L. Sawides, E. Gambra, and C. Dorronsoro, "Influence of adaptive-optics ocular aberration correction on visual acuity at different luminances and contrast polarities," J. Vis. **8**(13):1 (2008).
26. G. Osnabrugge, R. Horstmeyer, I. N. Papadopoulos, B. Judkewitz, and I. M. Vellekoop, "Generalized optical memory effect," Optica **4**, 886–892 (2017).